

Article

# Effect of Variable Thermal Conductivity and Magnetic Field for the Generated Photo-Thermal Waves on Microelongated Semiconductor

Abdulkafi M. Saeed <sup>1</sup>, Kh. Lotfy <sup>2,3,\*</sup> and Alaa A. El-Bary <sup>4</sup>

<sup>1</sup> Department of Mathematics, College of Science, Qassim University, P.O. Box 6644, Buraydah 51452, Saudi Arabia

<sup>2</sup> Department of Mathematics, Faculty of Science, Zagazig University, Zagazig P.O. Box 44519, Egypt

<sup>3</sup> Department of Mathematics, Faculty of Science, Taibah University, P.O. Box 344, Madinah 30002, Saudi Arabia

<sup>4</sup> Arab Academy for Science, Technology and Maritime Transport, Alexandria P.O. Box 1029, Egypt

\* Correspondence: khlotfy@zu.edu.eg

**Abstract:** A theoretical analysis of the dynamic impacts of a novel model in the microelongated-stimulated semiconductor medium is investigated. The influence of the magnetic field of the optically excited medium is taken into consideration according to the photothermal transport processes. The governing equations were created during the electronic (ED) and thermoelastic (TED) deformation processes. Thermal conductivity of the semiconductor microelongation medium is taken as temperature dependent. The interaction of thermal, microelongate, plasma, and mechanical waves is examined. Dimensionless formulae are used to solve the main equations in two dimensions (2D) using the harmonic wave method. The physical field equations have complete solutions when some conditions are applied to the semiconductor surface. The theoretical microelongated semiconductor model employed in this experiment was confirmed by comparing it to certain earlier studies. The numerical simulation for the principal physical field distributions is graphically displayed when silicon (Si) material is employed. The topic of the discussion was the impact of several factors, such as the magnetic field, thermal memory, and microelongation, on the propagation of waves for major fields.

**Keywords:** photo-generated; semiconductor; microelongation; magnetic field; carrier density; thermoelasticity

**MSC:** 74A15



**Citation:** Saeed, A.M.; Lotfy, K.; El-Bary, A.A. Effect of Variable Thermal Conductivity and Magnetic Field for the Generated Photo-Thermal Waves on Microelongated Semiconductor. *Mathematics* **2022**, *10*, 4270. <https://doi.org/10.3390/math10224270>

Academic Editors: Dimitrios Vlachos and George Kastis

Received: 17 October 2022

Accepted: 8 November 2022

Published: 15 November 2022

**Publisher's Note:** MDPI stays neutral with regard to jurisdictional claims in published maps and institutional affiliations.



**Copyright:** © 2022 by the authors. Licensee MDPI, Basel, Switzerland. This article is an open access article distributed under the terms and conditions of the Creative Commons Attribution (CC BY) license (<https://creativecommons.org/licenses/by/4.0/>).

## 1. Introduction

Recent years have seen increased acceptance of the photothermal (PT) technique as a helpful tool for analyzing the thermal and electrical properties of semiconductor materials. Due to its critical role in a variety of contemporary industries, such as sensors, solar cells, energy storage, cathodes of Li-O<sub>2</sub> batteries, energy conversion, and enhanced medical devices, semiconductors are a family of materials that have undergone recent intensive research. It is significant to highlight that the majority of renewable energy production requires knowledge of semiconductor nature. Substances that are insufficiently conductive and dielectric are known as semiconductors. When optical energy reaches a semiconductor material's surface, its intrinsic holes and electrons are activated, and the outcome is the development of electronic deformation (ED). Ghini et al. [1] explored novel energy storage methods that utilize green energies while maintaining self-sufficiency using metal oxide, which was prompted by the increased demand for self-powered devices nanocrystals. The excited electrons are propelled quickly to the surface by the thermal impact of light (optical energy), where they produce an electron cloud that is comparable

to convective density or plasma waves. Thermoelastic deformation (TED) is a modification of a material's internal structure brought on by photo-excitation and the ensuing heat effect [2]. The thermal excitation and transit of electrons result in mechanical (elastic) vibrations, and it is crucial to take into account how thermal conductivity alters as a result. As a result, the theory of thermoelasticity is utilized to research semiconductors in addition to the photothermal theory. The microinertia transport of the semiconductors' microelements should be taken into account with the internal changes predicted by ED and TED. According to Optoelectronics processes, many applications are investigated in solar cells using the optical properties of ZnS quantum dots [3]. On the other hand, Li et al. [4] used a combination of density functional theory (DFT) to explain the prospects of sensor performances of two-dimensional. Amouami et al. [5] studied the impact of geometrical shape according to the implementation of quantum dots to investigate the characteristic of dot solar cells.

Microelongation should be taken into account as the research of semiconductors progresses and becomes more dependent on the rotational movements (micro-deformation) of the interior particles [6]. Eringen [7,8] presented several theories that describe the micropolar theory of the internal particles of elastic bodies under the microstructure. The microstretch thermoelasticity theory has been introduced as a particular instance of the micromorphic theory. Numerous researchers have recently focused on the theory of microstretch thermoelasticity through the investigation of numerous theoretical applications [9–13]. The thermo-microstretch theory was utilized by Lotfy and Othman et al. [14] to analyze the propagation of waves through an elastic body. They did this by using the action of a magnetic field through a gravity field with starting stress. A hydromechanics viscoelastic porous medium's governing equations have been studied using the theory of thermo-microstretch by certain researchers [15,16]. The impact of diverse heat sources on a functionally graded microelongated elastic media was investigated [17,18] while accounting for the impact of microelongation parameters. According to the thermoelasticity theory, when the microelongated elastic media is taken into account under the influence of an internal heat source, Ailawalia et al. [19–21] investigated the plane strain deformation. However, Marin et al. [22–27] developed the micropolar and microstretch theories based on harmonic vibrations using the dipolar elastic bodies.

The first appearance of employing the photothermal theory occurred lately when a beam of laser beams was studied on a sample of a semiconductor material [28]. The photothermal technique was employed in photoacoustic spectroscopy (PAS) of semiconductor materials to comprehend the wave propagation characteristics of semiconductor materials [29]. Numerous contemporary electrical engineering applications for the usage of semiconductors in numerous sectors have evolved in the context of photothermal excitation techniques [30–32]. To examine the 2D deformation of thermoelastic interactions in semiconductors, Hobiny and Abbas [33] looked into the photothermal technique. The optically induced mechanism according to the ED in the context of the PAS approach for microcantilevers semiconducting was examined by Todorovic et al. [34,35]. Examining the overlap in the governing equations between the theories of thermoelasticity and photothermal. Lotfy et al. [36–40] investigated the thermal impact of light and laser on semiconductors. As a result, the photo-thermoelasticity theory was developed. When a polymer semiconductor material is utilized, the effect of the magnetic field with the Thomson effect is applied to explore the photo-thermoelasticity theory following the hyperbolic two-temperature theory [41–45]. LEDs and transistors are examples of semiconductors constructed of synthetic polymers. Such "conjugated polymers" are plastic substances that, when doped, transform from insulators to semiconductors [46].

When investigating semiconductors in the past, the majority of studies did not include the impact of microelongation parameters on the optical properties in addition to the impact of the magnetic field [41–45]. The current study proposes a novel model that, when microelongation properties of semiconductors are taken into consideration, describes the interaction between the thermoelastic theory and the photothermal theory. According to the

2D deformation, the impact of the magnetic field is also investigated on the microelongated semiconductor (TED and ED). The novel model, which is described as being dimensionless, is known as the photothermal-microelongated model. The harmonic waves technique is used to obtain the analytical solutions of the primary physical fields during optical excitation. According to some numerical simulations, the theoretical analysis outcomes are graphically displayed and assessed. The theoretical discussion addresses some parameters' primary effects.

**2. The Main Equations and Mathematical Model**

In this section, the Materials and Methods are described in sufficient detail. When a uniform magnetic field  $\vec{H} = (0, H_0, 0)$  in the direction of  $y$ -axial is applied to a microelongated stimulated semiconductor medium. The induced magnetic field  $\vec{h} = (0, h, 0)$  is created in this instance in the same direction. However, the induced electric field  $\vec{E} = (0, 0, E)$  is generated in the vertical direction, resulting in the current density  $\vec{J} = (J_x, J_y, J_z)$  (see Figure 1). According to a microelongated semiconductor medium that is flowing slowly and has a particle velocity of  $\vec{u}$ . In 2D,  $\vec{u} (= (u, 0, w) = u_i)$  is the displacement vector,  $u = u(x, z, t)$  and  $w = w(x, z, t)$  are the components of the displacement vector and the strain takes the form  $e = \frac{\partial u}{\partial x} + \frac{\partial w}{\partial z}$  (cubical dilatation). Since the electric permeability is  $\epsilon_0$  and the magnetic constant permeability is  $\mu_0$ , the linearized electromagnetic Maxwell's equations are written as follows:

$$\left. \begin{aligned} \vec{J} &= \vec{\nabla} \times \vec{h} - \epsilon_0 \dot{\vec{E}}, \\ \vec{\nabla} \times \vec{E} &= -\mu_0 \dot{H}, \\ \vec{E} &= -\mu_0 (\dot{\vec{u}} \times \vec{H}), \\ \vec{\nabla} \cdot \vec{H} &= 0, \\ \vec{h} &= H_0 (0, e, 0). \end{aligned} \right\} \tag{1}$$

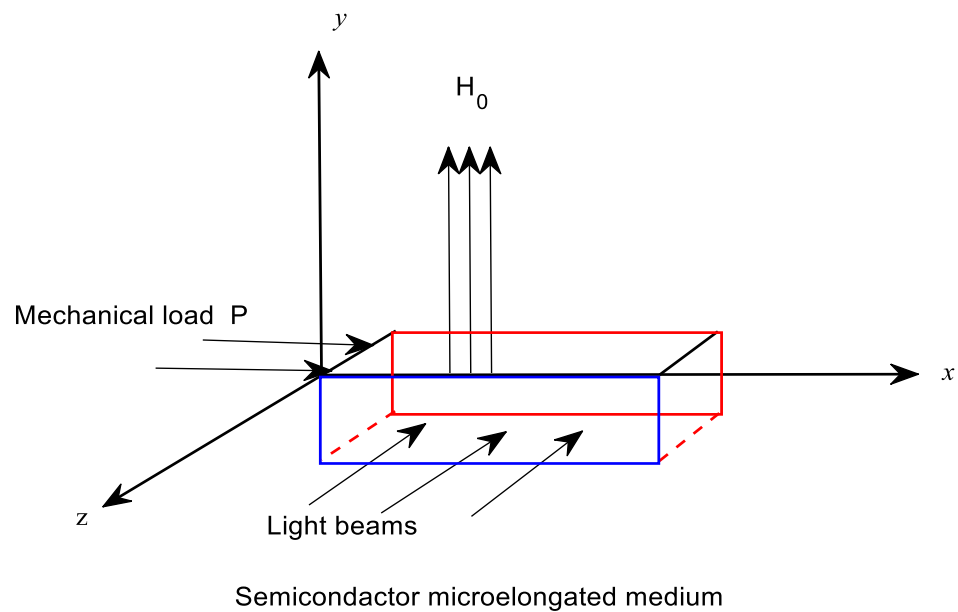


Figure 1. Geometry of the problem.

Using the elimination method, Equation (1) produces:

$$\left. \begin{aligned} E_x &= \mu_0 H_0 \dot{w}, E_y = 0, E_z = -\mu_0 H_0 \dot{u}, \\ J_x &= -\left(\frac{\partial h}{\partial z} + \mu_0 H_0 \varepsilon_0 \dot{w}\right), J_y = 0, J_z = \frac{\partial h}{\partial x} + \mu_0 H_0 \varepsilon_0 \dot{u}, \\ H_x &= 0, H_z = 0, H_y = H_0 + h(x, y, z), \\ \vec{F} &= \mu_0(\vec{J} \times \vec{H}) = (-\mu_0 H_0 \frac{\partial h}{\partial x} - \varepsilon_0 \mu_0^2 H_0^2 \frac{\partial^2 u}{\partial t^2}, 0, -\mu_0 H_0 \frac{\partial h}{\partial z} - \varepsilon_0 \mu_0^2 H_0^2 \frac{\partial^2 w}{\partial t^2}). \end{aligned} \right\} \quad (2)$$

Dot notation is used to represent the differentiation for time, where  $\vec{F} = \mu_0(\vec{J} \times \vec{H})$  is Lorentz's electromagnetic force. Utilizing the 2D Cartesian coordinates  $(x, 0, z)$  (see Figure 1), all main fields depend on  $(x, z, t)$ . The following present the other significant quantities in this work: the carrier density  $N(x, z, t)$  (plasma waves or carrier concentration, which measure the number of charge carriers per volume, in SI units; it is measured in  $m^{-3}$ ), the scalar microelongational function  $\varphi(x, z, t)$ , and the temperature  $T(x, z, t)$  (thermal waves). When the microelongated semiconductor medium is homogeneous, isotropic, and linear in this situation, the primary governing equations can be introduced following the microelongated photo-thermoelasticity theory as follows:

- (I) The constitutive relations for a microelongated semiconductor photo-thermoelastic medium have the following tensor form [17–21]:

$$\left. \begin{aligned} \sigma_{ij} &= (\lambda_o \varphi + \lambda u_{r,r}) \delta_{ij} + 2\mu u_{j,i} - \hat{\gamma}(1 + v_o \frac{\partial}{\partial t}) T \delta_{ij} - ((3\lambda + 2\mu) d_n N) \delta_{ij}, \\ m_i &= a_o \varphi_{,i}, \\ s - \sigma &= \lambda_o u_{i,i} - \beta_1 (1 + v_o \frac{\partial}{\partial t}) T + -((3\lambda + 2\mu) d_n N) \delta_{2i} + \lambda_1 \varphi. \end{aligned} \right\} \quad (3)$$

where the comma notation followed by a subscript denotes partial differentiation with respect to the corresponding coordinates.

- (II) The equations for thermal waves and plasma waves are [28]:

$$\dot{N} = D_E N_{,ii} - \frac{N}{\tau} + \kappa T \quad (4)$$

- (III) The motion equation affected by the electromagnetic field and the semiconductor medium's microelongation equation with the microelongation and microinertia processes are found in [45,46]:

$$(\lambda + \mu) u_{j,ij} + \mu u_{i,jj} + \lambda_o \varphi_{,i} - \hat{\gamma}(1 + v_o \frac{\partial}{\partial t}) T_{,i} - \delta_n N_{,i} + \vec{F} = \rho \ddot{u}_i \quad (5)$$

$$\alpha_o \varphi_{,ii} - \lambda_1 \varphi - \lambda_o u_{j,j} + \hat{\gamma}_1 (1 + v_o \frac{\partial}{\partial t}) T = \frac{1}{2} j \rho \ddot{\varphi} \quad (6)$$

- (IV) According to the interplay of optical, thermal, elastic, and microelongation waves, the general version of the heat Equation is [23]:

$$(KT_{,i})_{,i} - \rho C_E (n_1 + \tau_o \frac{\partial}{\partial t}) \dot{T} - \hat{\gamma} T_o (n_1 + n_o \tau_o \frac{\partial}{\partial t}) \dot{u}_{i,i} + \frac{E_g}{\tau} N = \hat{\gamma}_1 T_o \dot{\varphi} \quad (7)$$

where  $\kappa = \frac{\partial n_o}{\partial T} \frac{T}{\tau}$  denotes the coupling thermal activation parameter in the case of temperature change, and  $\alpha_{t_2}$  is the coefficient of the microelongational linear thermal expansions,  $\hat{\gamma}_1 = (3\lambda + 2\mu) \alpha_{t_2}$  is the microelongational thermal expansion, and  $n_1$  and  $n_o$  are two chosen constants. In Equation (7), the third component quantifies the heat produced by stress waves, whereas the second term on the right side characterizes the effect of heat generation by the sample's carrier volume and surface de-excitations. The third and fourth terms in the elastic Equation (5), respectively, describe the

source term and the effect of the thermal wave and plasma wave on the elastic wave. Equations (4) through (7) in the 2D deformations can be generally recast as [46]:

$$\left. \begin{aligned} &(\lambda + \mu) \left( \frac{\partial^2 u}{\partial x^2} + \frac{\partial^2 w}{\partial x \partial z} \right) + \mu \left( \frac{\partial^2 u}{\partial x^2} + \frac{\partial^2 u}{\partial z^2} \right) + \lambda_o \frac{\partial \varphi}{\partial x} \\ & - \hat{\gamma} \left( 1 + v_o \frac{\partial}{\partial t} \right) \frac{\partial T}{\partial x} - \delta_n \frac{\partial N}{\partial x} - \mu_0 H_0 \frac{\partial h}{\partial x} - \epsilon_0 \mu_0^2 H_0^2 \frac{\partial^2 u}{\partial t^2} = \rho \left( \frac{\partial^2 u}{\partial t^2} \right) \end{aligned} \right\} \quad (8)$$

$$\left. \begin{aligned} &(\lambda + \mu) \left( \frac{\partial^2 u}{\partial x \partial z} + \frac{\partial^2 w}{\partial z^2} \right) + \mu \left( \frac{\partial^2 w}{\partial x^2} + \frac{\partial^2 w}{\partial z^2} \right) + \lambda_o \frac{\partial \varphi}{\partial z} \\ & - \hat{\gamma} \left( 1 + v_o \frac{\partial}{\partial t} \right) \frac{\partial T}{\partial z} - \delta_n \frac{\partial N}{\partial z} - \mu_0 H_0 \frac{\partial h}{\partial z} - \epsilon_0 \mu_0^2 H_0^2 \frac{\partial^2 w}{\partial t^2} = \rho \left( \frac{\partial^2 w}{\partial t^2} \right) \end{aligned} \right\} \quad (9)$$

$$\alpha_o \left( \frac{\partial^2 \varphi}{\partial x^2} + \frac{\partial^2 \varphi}{\partial z^2} \right) - \lambda_1 \varphi - \lambda_o e + \hat{\gamma}_1 \left( 1 + v_o \frac{\partial}{\partial t} \right) T = \frac{1}{2} j \rho \frac{\partial^2 \varphi}{\partial t^2} \quad (10)$$

$$\left. \begin{aligned} &\left( K(T) \left( \frac{\partial T}{\partial x} + \frac{\partial T}{\partial z} \right) \right)_{,i} - \rho C_E \left( n_1 + \tau_o \frac{\partial}{\partial t} \right) \frac{\partial T}{\partial t} - \hat{\gamma} T_o \left( n_1 + n_o \tau_o \frac{\partial}{\partial t} \right) \frac{\partial e}{\partial t} + \frac{E_s}{\tau} N = \\ & \hat{\gamma}_1 T_o \frac{\partial \varphi}{\partial t} \end{aligned} \right\} \quad (11)$$

It is possible to select the thermal conductivity of a microelongated semiconductor material as a variable case, which can be expressed as a linear function of temperature. According to the thermal effect of light beams in this situation, the thermal conductivity can be expressed as follows [36,37]:

$$K(T) = K_0(1 + K_1 T) \quad (12)$$

The kind of thermal conductivity is determined by the non-positive parameter  $K_1 \leq 0$ . When the medium is independent of temperature, the physical constant  $K_0$  (reference) is thermal conductivity. To convert the nonlinear terms in the thermal conductivity equation into linear terms, one can use the integral form of Kirchhoff’s theory of temperature [45].

$$\Theta = \frac{1}{K_0} \int_0^T K(\vartheta) d\vartheta \quad (13)$$

where  $\kappa = \frac{\partial n_0}{\partial T} \frac{T}{\tau}$  is the parameter controlling the coupling’s thermal activation ( $n_0$  represents the equilibrium carrier concentration). Equations (6) and (7), which fulfill the following differentiation relations, can be used to include the variable thermal conductivity in calculations:

$$\left. \begin{aligned} &K_0 \Theta_{,i} = K(T) T_{,i}, \quad \text{also } K_0 \frac{\partial \Theta}{\partial t} = K(T) \frac{\partial T}{\partial t}, \\ &\frac{K_0}{K(T)} \Theta_{,i} = T_{,i}, \\ &K_0 \Theta_{,ii} = (K(T) T_{,i})_{,i}. \end{aligned} \right\} \quad (14)$$

If the map transform and differentiation impacts are used, Equation (2) can be rewritten as follows:

$$\left. \begin{aligned} &\frac{\partial}{\partial t} \frac{\partial N}{\partial x_j} = D_E \frac{\partial N_{,ii}}{\partial x_j} - \frac{1}{\tau} \frac{\partial N}{\partial x_j} + \kappa \frac{\partial T}{\partial x_j} \Rightarrow \\ &\frac{\partial}{\partial t} \frac{\partial N}{\partial x_j} = D_E \frac{\partial N_{,ii}}{\partial x_j} - \frac{1}{\tau} \frac{\partial N}{\partial x_j} + \frac{\kappa K_0}{K} \frac{\partial \Theta}{\partial x_j} \Rightarrow \\ &\frac{\partial}{\partial t} \frac{\partial N}{\partial x_j} = D_E \frac{\partial N_{,ii}}{\partial x_j} - \frac{1}{\tau} \frac{\partial N}{\partial x_j} + \kappa \frac{\partial \Theta}{\partial x_j}. \end{aligned} \right\} \quad (15)$$

where the non-linear terms were disregarded, and the Taylor expansion was applied to the final term in the preceding Equation (13), as follows:

$$\begin{aligned} \frac{\kappa K_0}{K} \frac{\partial \Theta}{\partial x_j} &= \frac{\kappa K_0}{K_0(1+K_1 T)} \frac{\partial \Theta}{\partial x_j} = \kappa(1 + K_1 T)^{-1} \frac{\partial \Theta}{\partial x_j} = \kappa(1 - K_1 T + (K_1 T)^2 - \dots) \frac{\partial \Theta}{\partial x_j} = \\ & \kappa \frac{\partial \Theta}{\partial x_j} - \kappa K_1 T \frac{\partial \Theta}{\partial x_j} + (K_1 T)^2 \frac{\partial \Theta}{\partial x_j} - \dots = \kappa \frac{\partial \Theta}{\partial x_j} \end{aligned} \quad (16)$$

Integrating Equation (15) to spatial coordinates  $x_i$  results in:

$$\frac{\partial N}{\partial t} = D_E N_{,ii} - \frac{1}{\tau} N + \kappa \Theta. \tag{17}$$

However, the map Equation (7) can rewrite the microelongated Equation (5) as shown below:

$$\Theta_{,ii} - \frac{1}{k} (n_1 + \tau_o \frac{\partial}{\partial t}) \frac{\partial \Theta}{\partial t} - \frac{\hat{\gamma} T_o}{K_0} (n_1 + n_o \tau_o \frac{\partial}{\partial t}) \dot{u}_{i,i} + \frac{E_g}{K_0 \tau} N = \frac{\hat{\gamma}_1 T_0}{K_0} \dot{\varphi} \tag{18}$$

where the thermal diffusivity is  $\frac{1}{k} = \frac{\rho C_E}{K_0}$ .

The values of the parameters  $n_o$  and  $n_1$  can be chosen based on the photo-thermoelasticity models (selected constants). On the other hand, the thermal memories determine the coupled-dynamical model (CD), Green and Lindsay (GL), and Lord and Shulman (LS) models or determine the types of microelongated photo-thermoelasticity models [45–47]. The following dimensionless quantities can be used to present the main equations in a condensed manner:

$$\left. \begin{aligned} \bar{N} &= \frac{\delta_n}{2\mu+\lambda} N, (\bar{x}_i, \bar{u}_i) = \frac{1}{\omega^* C_T} (x_i, u_i), (\bar{t}, \bar{\tau}_o, \bar{v}_o) = \frac{(t, \tau_o, v_o)}{\omega^*}, \\ C_T^2 &= \frac{2\mu+\lambda}{\rho}, \bar{\Theta} = \frac{\hat{\gamma} \Theta}{2\mu+\lambda}, \bar{\sigma}_{ij} = \frac{\sigma_{ij}}{2\mu+\lambda}, \bar{\varphi} = \frac{\rho C_T^2}{T_o \hat{\gamma}} \varphi, \omega^* = \frac{K_0}{\rho C_E C_T^2}, \\ (\Pi', \psi') &= \frac{(\Pi, \psi)}{(C_T \omega^*)^2}, C_L^2 = \frac{\mu}{\rho}, h' = \frac{h}{H_0}. \end{aligned} \right\} \tag{19}$$

The main equations using the dimensionless Equation (19) can be written as follows (remove the superscripts to write the equations in a simple form (for convenience)):

$$(\nabla^2 - \varepsilon_3 - \varepsilon_2 \frac{\partial}{\partial t}) N + \varepsilon_4 \Theta = 0 \tag{20}$$

$$\left. \begin{aligned} \frac{\partial^2 u}{\partial t^2} &= \frac{(\lambda+\mu)}{\rho C_T^2} \frac{\partial e}{\partial x} + \frac{\mu}{\rho C_T^2} \nabla^2 u + \frac{T_o \hat{\gamma} \lambda_o}{(\rho C_T^2)^2} \frac{\partial \varphi}{\partial x} - (1 + v_o \frac{\partial}{\partial t}) \frac{\partial \Theta}{\partial x} - \\ &\frac{\partial N}{\partial x} - \frac{\mu_0 H_0^2}{\rho \omega^* C_T} \frac{\partial h}{\partial x} - \frac{\varepsilon_0 \mu_0^2 H_0^2}{\rho} \frac{\partial^2 u}{\partial t^2} \end{aligned} \right\} \tag{21}$$

$$\left. \begin{aligned} \frac{\partial^2 w}{\partial t^2} &= \frac{(\lambda+\mu)}{\rho C_T^2} \frac{\partial e}{\partial z} + \frac{\mu}{\rho C_T^2} \nabla^2 w + \frac{T_o \hat{\gamma} \lambda_o}{(\rho C_T^2)^2} \frac{\partial \varphi}{\partial z} - (1 + v_o \frac{\partial}{\partial t}) \frac{\partial \Theta}{\partial z} - \\ &\frac{\partial N}{\partial z} - \frac{\mu_0 H_0^2}{\rho \omega^* C_T} \frac{\partial h}{\partial z} - \frac{\varepsilon_0 \mu_0^2 H_0^2}{\rho} \frac{\partial^2 w}{\partial t^2} \end{aligned} \right\} \tag{22}$$

$$(\nabla^2 - C_3 - C_4 \frac{\partial^2}{\partial t^2}) \varphi - C_5 e + C_6 (1 + v_o \frac{\partial}{\partial t}) \Theta = 0 \tag{23}$$

$$\nabla^2 T - (n_1 + \tau_o \frac{\partial}{\partial t}) \frac{\partial \Theta}{\partial t} - \varepsilon (n_1 + n_o \tau_o \frac{\partial}{\partial t}) \frac{\partial e}{\partial t} + \varepsilon_5 N = \varepsilon_1 \frac{\partial \varphi}{\partial t} \tag{24}$$

Helmholtz’s theory is applied for further simplification, and the displacement components can be expressed as follows in terms of the vector space–time function  $\Psi(x, z, t) = (0, \psi, 0)$  and potential scalar function  $\Pi(x, z, t)$ :

$$\vec{u} = grad \Pi + curl \Psi, u = \frac{\partial \Pi}{\partial x} - \frac{\partial \psi}{\partial z}, w = \frac{\partial \Pi}{\partial z} + \frac{\partial \psi}{\partial x} \tag{25}$$

Equation (18) substituted for the primary Equations (14)–(17) results in:

$$(\alpha \nabla^2 - \mathbb{R}_H \frac{\partial^2}{\partial t^2}) \Pi + (1 + v_o \frac{\partial}{\partial t}) \Theta + a_1 \varphi - N = 0, \tag{26}$$

$$(\nabla^2 - \mathbb{R}_H a_3 \frac{\partial^2}{\partial t^2}) \psi = 0, \tag{27}$$

$$(\nabla^2 - C_3 - C_4 \frac{\partial^2}{\partial t^2})\varphi - C_5 \nabla^2 \Pi + C_6(1 + v_0 \frac{\partial}{\partial t})\Theta = 0 \tag{28}$$

$$\left( \nabla^2 - (n_1 \frac{\partial}{\partial t} + \tau_0 \frac{\partial^2}{\partial t^2}) \right) \Theta - \varepsilon(n_1 \frac{\partial}{\partial t} + n_0 \tau_0 \frac{\partial^2}{\partial t^2}) \nabla^2 \Pi + \varepsilon_5 N - \varepsilon_1 \frac{\partial \varphi}{\partial t} = 0 \tag{29}$$

On the other hand, it is possible to derive the constitutive Equations (3) for 2D deformation as follows [33,35]:

$$\left. \begin{aligned} \sigma_{xx} &= \frac{\partial u}{\partial x} + a_2 \frac{\partial w}{\partial z} - (1 + v_0 \frac{\partial}{\partial t}) \Theta - N + a_1 \varphi, \\ \sigma_{zz} &= a_2 \frac{\partial u}{\partial x} + \frac{\partial w}{\partial z} - (1 + v_0 \frac{\partial}{\partial t}) \Theta - N + a_1 \varphi, \\ \sigma_{xz} &= a_4 \left( \frac{\partial u}{\partial z} + \frac{\partial w}{\partial x} \right). \end{aligned} \right\} \tag{30}$$

where

$$\begin{aligned} a_1 &= \frac{T_0 \hat{\gamma} \lambda_0}{(\rho C_T^2)^2}, a_2 = \frac{\lambda}{\rho C_T^2}, a_3 = \frac{\rho C_T^2}{\mu}, \varepsilon = \frac{\hat{\gamma}^2 \omega^* T_0}{K_0 \rho}, \varepsilon_1 = \frac{\hat{\gamma}_1 \hat{\gamma}^2 \omega^* T_0}{K_0 \rho (2\mu + \lambda)}, \varepsilon_2 = \frac{\omega^* C_T^2}{D_E}, a_4 = \frac{\mu}{\rho C_T^2}, \\ C_4 &= \frac{\rho j C_T^2}{2\alpha_0}, \varepsilon_3 = \frac{\omega^{*2} C_T^2}{\tau D_E}, \varepsilon_4 = \frac{\kappa d_n \omega^{*2} \rho}{D_E \alpha_{H1}}, \varepsilon_5 = \frac{E_g \hat{\gamma} \omega^{*2} C_T^2}{\tau K_0 \delta_n}, C_3 = \frac{\lambda_1 C_T^2 \omega^{*2}}{\alpha_0}, \\ C_5 &= \frac{\lambda_0 \rho C_T^4 \omega^{*2}}{\alpha_0 T_0 \hat{\gamma}}, C_6 = \frac{\hat{\gamma}_1 \rho \omega^{*2} T_0}{\hat{\gamma} \alpha_0}, \mathbb{R}_H = 1 + \varepsilon_0 \mu_0^2 H_0^2 / \rho, \alpha = 1 + \frac{\mu_0 H_0^2}{\rho \omega^* C_T}. \end{aligned}$$

The symbol  $\varepsilon_1, \varepsilon_5, \varepsilon_4$  are the coupling thermoelastic, coupling thermo-energy, and thermo-electric parameters, and  $\mathbb{R}_H$  is the electromagnetic number that refers to the effect of the external magnetic field.

### 3. Analyze Harmonic Waves

The harmonic wave method that is used to find comprehensive solutions in 2D for the fundamental fields is what drives the normal mode analysis. For a function  $f(x, z, t)$ , the solutions for harmonic waves can be written as follows [47–49]:

$$f(x, z, t) = \bar{f}(x) \exp(\omega t + ibz). \tag{31}$$

The function  $\bar{f}(x)$  expresses the amplitude of  $f(x, y, t)$ ,  $i = \sqrt{-1}$ ,  $b$  is the wave number and  $\omega = \omega_0 + i\zeta$  denotes the complex time-frequency. Equation (24) from the normal mode approach is applied to Equations (20) and (26)–(29), resulting in:

$$(D^2 - \alpha_1)\bar{N} + \varepsilon_4 \bar{\Theta} = 0, \tag{32}$$

$$(\alpha D^2 - A_1)\bar{\Pi} + A_2 \bar{\Theta} + a_1 \bar{\varphi} - \bar{N} = 0, \tag{33}$$

$$(D^2 - A_3)\bar{\psi} = 0, \tag{34}$$

$$(D^2 - A_4)\bar{\varphi} - C_5(D^2 - b^2)\bar{\Pi} + A_5 \bar{\Theta} = 0, \tag{35}$$

$$(D^2 - A_6)\bar{\Theta} - A_7(D^2 - b^2)\bar{\Pi} + \varepsilon_5 \bar{N} - A_8 \bar{\varphi} = 0 \tag{36}$$

$$\left. \begin{aligned} \bar{\sigma}_{xx} &= D\bar{u} + iba_2 \bar{w} - A_2 \bar{\Theta} - \bar{N} + a_1 \bar{\varphi}, \\ \bar{\sigma}_{zz} &= a_2 D\bar{u} + ib\bar{w} - A_2 \bar{\Theta} - \bar{N} + a_1 \bar{\varphi}, \\ \bar{\sigma}_{xz} &= a_4 (ib\bar{u} + D\bar{w}). \end{aligned} \right\} \tag{37}$$

where

$$\left. \begin{aligned} \alpha_1 &= b^2 + \varepsilon_3 + \varepsilon_2 \omega, A_1 = \alpha b^2 + \mathbb{R}_H \omega^2, A_2 = 1 + v_0 \omega, A_3 = b^2 + \mathbb{R}_H a_3 \omega^2, \\ D &= \frac{d}{dx}, A_4 = b^2 + C_3 + C_4 \omega^2, A_5 = C_6(1 + v_0 \omega), \\ A_6 &= b^2 + \omega(n_1 + \tau_0 \omega), A_7 = \varepsilon(n_1 \omega + n_0 \tau_0 \omega^2), A_8 = \varepsilon_1 \omega. \end{aligned} \right\} \tag{38}$$

The elimination method for the functions  $\bar{\varphi}, \bar{N}, \bar{T}$  and  $\bar{\Pi}$  is used to solve the system of Equations (32), (33), and (35). Equations (35) and (36) to produce the following solution:

$$\{D^8 - C_1D^6 + C_2D^4 - C_3D^2 + C_4\}(\bar{\varphi}, \bar{N}, \bar{\Theta}, \bar{\Pi}) = 0 \tag{39}$$

where

$$\begin{aligned} C_1 &= -(-A_2A_7 + C_5a_1 - A_1 - A_4 - A_6 - \alpha_1)\alpha^{-1}, \\ C_2 &= \left( \begin{aligned} &(A_2A_7 - C_5a_1 + A_1 + A_4 + A_6)\alpha_1 + (A_7 - \varepsilon_3)\varepsilon_4 + \\ &(b^2A_7 + A_4A_7 - A_8)A_2 - b^2C_5a_1 - A_5A_7a_1 - A_6C_5a_1 - A_1A_4 + A_1A_6 + A_4A_6 \end{aligned} \right)\alpha^{-1}, \\ C_3 &= \left( \begin{aligned} &-((-A_2A_7 + C_5a_1)b^2 - A_2A_4A_7 + A_5A_7a_1 + A_6C_5a_1 - A_1A_4 - A_1A_6 + A_2A_8 - A_4A_6)\alpha_1 \\ &(-C_5a_1 + A_1 + A_4)\varepsilon_4\varepsilon_3 + (-b^2A_7a_2 - A_4A_7a_2 + A_8)\varepsilon_4 + (-A_2A_4A_7 + A_5A_7a_1 + \\ &A_6C_5a_1)b^2 - A_1A_4A_6 + A_2A_4A_8 - A_5A_8a_1 \end{aligned} \right)\alpha^{-1}, \\ C_4 &= \left( \begin{aligned} &((b^2C_5a_1 - A_1A_4)\varepsilon_3 + b^2A_4A_7 - A_4A_8)\varepsilon_4 + \\ &((A_2A_4A_7 - A_5A_7 - A_6C_5a_1)b^2 + A_1A_4A_6 - A_2A_4A_8 + A_5A_8a_1)\alpha_1 \end{aligned} \right)\alpha^{-1}. \end{aligned}$$

The decomposition (factorization) of the ordinary differential Equation (39) is as follows:

$$(D^2 - k_1^2)(D^2 - k_2^2)(D^2 - k_3^2)(D^2 - k_4^2)\{\bar{\Theta}, \bar{N}, \bar{\Pi}, \bar{\varphi}\}(x) = 0 \tag{40}$$

The quantities  $k_n^2 (n = 1, 2, 3, 4)$  represent the roots of the characteristic equation.

The following formulation can be used to represent the linear general solutions of Equation (39) for the key fields:

$$\bar{\Theta}(x) = \sum_{i=1}^4 Q_i(b, \omega)e^{-k_i x} \tag{41}$$

$$\bar{\varphi}(x) = \sum_{i=1}^4 Q'_i(b, \omega)e^{-k_i x} = \sum_{i=1}^4 h_{1i}Q_i(b, \omega)e^{-k_i x}, \tag{42}$$

$$\bar{\Pi}(x) = \sum_{i=1}^4 Q''_i(b, \omega)e^{-k_i x} = \sum_{i=1}^4 h_{2i}Q_i(b, \omega)e^{-k_i x}, \tag{43}$$

$$\bar{N}(x) = \sum_{i=1}^4 Q'''_i(b, \omega)e^{-k_i x} = \sum_{i=1}^4 h_{3i}Q_i(b, \omega)e^{-k_i x}. \tag{44}$$

where  $Q_i \ i = 1, 2, 3, 4, Q'''_i, Q'_i$  and  $Q''_i$  are unspecific parameters.

$$\begin{aligned} h_{1i} &= \frac{(d_1k_i^4 + d_2k_i^2 + d_3)}{(k_i^6 + d_4k_i^4 + d_5k_i^2 + d_6)}, h_{3i} = -\frac{(\varepsilon_4)}{(k_i^2 - \alpha_1)}, h_{2i} = \frac{(A_2k_i^4 + d_7k_i^2 + d_8)}{(k_i^6 + d_4k_i^4 + d_5k_i^2 + d_6)}, \\ d_1 &= A_2C_5 - A_5, d_2 = -A_2b^2C_5 - A_2C_5\alpha_1 - C_5a_2\varepsilon_4 + A_1A_5 + A_5\alpha_1, \\ d_3 &= b^2A_2C_5\alpha_1 + b^2C_5a_2\varepsilon_4 - A_1A_5\alpha_1, d_4 = C_5a_1 - A_1 - A_4 - \alpha_1, \\ d_5 &= -b^2C_5a_1 - C_5a_1\alpha_1 + A_1A_4 + A_1\alpha_1 + A_4\alpha_1, d_6 = b^2\alpha_1a_1C_5 - A_1A_4\alpha_1, \\ d_7 &= -A_2A_4 - A_2\alpha_1 + A_5a_1 - a_2\varepsilon_4, d_8 = A_2A_4\alpha_1 + A_4a_2\varepsilon_4 - a_1A_5\alpha_1. \end{aligned}$$

However, Equation (34) can be broken down into the following parts:

$$(D^2 - k_5^2)\bar{\psi}(x) = 0 \tag{45}$$

where  $k_5^2$ , the fifth root of Equation (34), has the following form:

$$k_5 = \pm\sqrt{A_3} = \pm\omega\sqrt{a_3} \tag{46}$$

Equation (45), when resolved, yields:

$$\bar{\psi}(x) = \mathbb{Q}_5(b, \omega) \exp(-k_5x) \tag{47}$$

When the normal mode analysis is used, the displacement components (elastic waves) and the stress (mechanical waves) components can be recast terms  $\mathbb{Q}_i$  according to Equations (25) and (30), respectively.

$$\bar{u}(x) = -\sum_{i=1}^4 \mathbb{Q}_i h_{2i} k_i e^{-k_i x} - ib\mathbb{Q}_5 e^{-k_5 x}, \quad \bar{w}(x) = \sum_{i=1}^4 ibh_{2i} \mathbb{Q}_i e^{-k_i x} - k_5 \mathbb{Q}_5 e^{-k_5 x} \tag{48}$$

$$\left. \begin{aligned} \bar{\sigma}_{xx} &= \sum_{n=1}^4 \mathbb{Q}_n (h_{2i}(k_n^2 - b^2 a_2) - A_2 - h_{3i} + a_1 h_{1i}) e^{-k_n x} - ibk_5 (a_2 - 1) \mathbb{Q}_5 e^{-k_5 x}, \\ \bar{\sigma}_{zz} &= \sum_{n=1}^4 \mathbb{Q}_n (h_{2i}(a_2 k_n^2 - b^2) - A_2 - h_{3i} + a_1 h_{1i}) e^{-k_n x} - ibk_5 (1 - a_2) \mathbb{Q}_5 e^{-k_5 x}, \\ \bar{\sigma}_{xz} &= \sum_{n=1}^4 ib\mathbb{Q}_n k_n (h_{2i} - 1) e^{-k_n x} + (1 + k_5^2) \mathbb{Q}_5 e^{-k_5 x}. \end{aligned} \right\} \tag{49}$$

where the roots can be chosen in the positive real form  $\text{Re}(k_n) > 0$ .

#### 4. Boundary Conditions

To achieve the whole solution, unknown parameters  $\mathbb{Q}_n$  must be identified. The outer microelongated semiconductor surface (at  $x = 0$ ) is subjected to a few conditions in this instance [50].

At  $x = 0$ , the following mechanical loads with load pressure  $P$  conditions under harmonic wave analysis can be taken (Figure 1):

$$\left. \begin{aligned} \sigma_{xx} = -P &\Rightarrow \bar{\sigma}_{xx} = -\bar{p} \exp(\omega t + ibz), \\ P(x, z, t) &= \bar{p}(x) \exp(\omega t + ibz) \end{aligned} \right\} \tag{50}$$

The other mechanical condition for the tangent stress component can be chosen as a traction free

$$\sigma_{xz} = 0 \Rightarrow \bar{\sigma}_{xz} = 0, \text{ at } x = 0. \tag{51}$$

In a thermally isolated application that has the following formulation, the thermal condition at  $x = 0$  is chosen:

$$\frac{\partial \Theta}{\partial x} = 0 \Rightarrow \frac{d\bar{\Theta}}{dx} = 0 \tag{52}$$

The elongation case for the microelongation condition at the free surface is derived at negative elongation function  $\phi$  as:

$$\bar{\varphi} = -\phi \tag{53}$$

Recombination operations can be used to determine the carrier density condition, which can be used to estimate the electron concentration and velocity at  $x = 0$  as:

$$\frac{d\bar{N}}{dx} = -\frac{\tilde{s}n_0}{D_E} \tag{54}$$

The following relationships can be recast as follows, using Equations (50)–(53) and the values of  $\bar{T}, \bar{\sigma}_{xx}, \bar{\sigma}_{xz}, \bar{\varphi}$ , and:

$$\left. \begin{aligned} \sum_{n=1}^4 \mathbb{Q}_n (h_{2i}(k_n^2 - b^2 a_2) - A_2 - h_{3i} + a_1 h_{1i}) - ibk_5 (a_2 - 1) \mathbb{Q}_5 &= -\bar{p} \exp(\omega t + ibz), \\ \sum_{n=1}^4 ib\mathbb{Q}_n k_n (h_{2i} - 1) + (1 + k_5^2) \mathbb{Q}_5 &= 0. \end{aligned} \right\} \tag{55}$$

$$\sum_{i=1}^4 -k_i Q_i(b, \omega) = 0, \sum_{i=1}^4 h_{1i} Q_i(b, \omega) = 0, \sum_{i=1}^4 h_{3i} k_i Q_i(b, \omega) = \frac{\tilde{s}n_0}{D_E} \tag{56}$$

When the parameters  $Q_n$  are definite while solving the system of Equations (54) and (55), complete solutions are found.

**5. Validation**

*5.1. Generalized Microelongation Thermoelasticity Theory*

When the plasma wave’s carrier density  $N(x, y, t)$  is disregarded (i.e.,  $N = 0$ ), the microelongation magneto-thermoelasticity theory is produced without consideration of optical energy. The governing Equations (2)–(5) are reduced to [16,17] in this situation:

$$\left. \begin{aligned} (\lambda + \mu)u_{j,ij} + \mu u_{i,jj} + \lambda_o \varphi_{,i} - \hat{\gamma} (1 + v_o \frac{\partial}{\partial t}) T_{,i} + \vec{F} &= \rho \ddot{u}_i, \\ \alpha_o \varphi_{,ii} - \lambda_1 \varphi - \lambda_o u_{j,j} + \hat{\gamma}_1 (1 + v_o \frac{\partial}{\partial t}) T &= \frac{1}{2} j \rho \ddot{\varphi}, \\ (KT_{,i})_{,i} - \rho C_E (n_1 + \tau_o \frac{\partial}{\partial t}) \dot{T} - \hat{\gamma} T_o (n_1 + n_o \tau_o \frac{\partial}{\partial t}) \dot{u}_{i,i} &= \hat{\gamma}_1 T_o \dot{\varphi}. \end{aligned} \right\} \tag{57}$$

*5.2. The Generalized Theory of Photothermoelasticity*

The magneto-photo-thermoelasticity theory is obtained when the elongation parameters are ignored ( $\alpha_o = \lambda_o = \lambda_1 = 0$ ). Equations (2)–(5) of the system are reduced to:

$$\left. \begin{aligned} \dot{N} &= D_E N_{,ii} - \frac{N}{\tau} + \kappa T, \\ (\lambda + \mu)u_{j,ij} + \mu u_{i,jj} - \hat{\gamma} (1 + v_o \frac{\partial}{\partial t}) T_{,i} - \delta_n N_{,i} + \vec{F} &= \rho \ddot{u}_i, \\ (KT_{,i})_{,i} - \rho C_E (n_1 + \tau_o \frac{\partial}{\partial t}) \dot{T} - \hat{\gamma} T_o (n_1 + n_o \tau_o \frac{\partial}{\partial t}) \dot{u}_{i,i} + \frac{E_g}{\tau} N &= 0. \end{aligned} \right\} \tag{58}$$

This issue is investigated by [28,30].

*5.3. Different Magneto-Photo-Thermoelasticity Models for Microelongation*

According to the various values of the thermal memory ( $\tau_o, v_o$ ) and the constants  $n_1$  and  $n_o$ , the various models in this work can be obtained as follows [49]:

- (I) When  $n_1 = 1, n_o = \tau_o = v_o = 0$ , the coupled thermoelasticity (CD) model was visible [49].
- (II) When  $n_1 = n_o = 1, v_o = 0, \tau_o > 0$ , the Lord and Shulman (LS) model was visible [48].
- (III) When  $n_1 = 1, n_o = 0, v_o \geq \tau_o > 0$ , the Green and Lindsay (GL) model was visible [47].

*5.4. The Variable Thermal Conductivity*

When the negative parameter is ignored,  $K_1 = 0$ , and the microelongated semiconductor medium is independent of the gradient temperature,  $K = K_0$ . In this instance, the issue is investigated when thermal conductivity is constant while considering the effects of the magnetic field.

*5.5. Influence of Electromagnetic Field*

The induced magnetic field and induced electric field are also disregarded when the effect of a uniform magnetic field is disregarded ( $H_0 = 0$ ). When the thermal conductivity changes without a magnetic field, Lorentz’s electromagnetic force disappears in this situation, and the system explains the microelongation photo-thermoelasticity hypothesis.

The relationship between  $T$  and  $\Theta$  can be discovered under the map transform, which is described in Equations (6) and (7) as follows:

$$\Theta = \frac{1}{K_0} \int_0^T K_0 (1 + K_1 T) dT = T + \frac{K_1}{2} T^2 = \frac{K_1}{2} (T + \frac{1}{K_1})^2 - \frac{1}{2K_1} \tag{59}$$

$$T = \frac{1}{K_1} \left[ \sqrt{1 + 2K_1\Theta} - 1 \right] = \frac{1}{K_1} \left[ \sqrt{1 + 2K_1\Theta \exp(\omega t + ibz)} - 1 \right] \tag{60}$$

### 6. Discussion and Numerical Outcomes

This section simulates the wave propagation of the primary fields within the microelongated semiconductor medium. The physical constants of silicon (Si) are utilized as an example of a semiconductor medium to carry out this simulation numerically. This numerical simulation was completed graphically using MATLAB (2022a) on a personal computer. The physical constants entered for silicon material are as follows in Table 1 [50,51].

**Table 1.** The physical input parameters of Si medium in SI units.

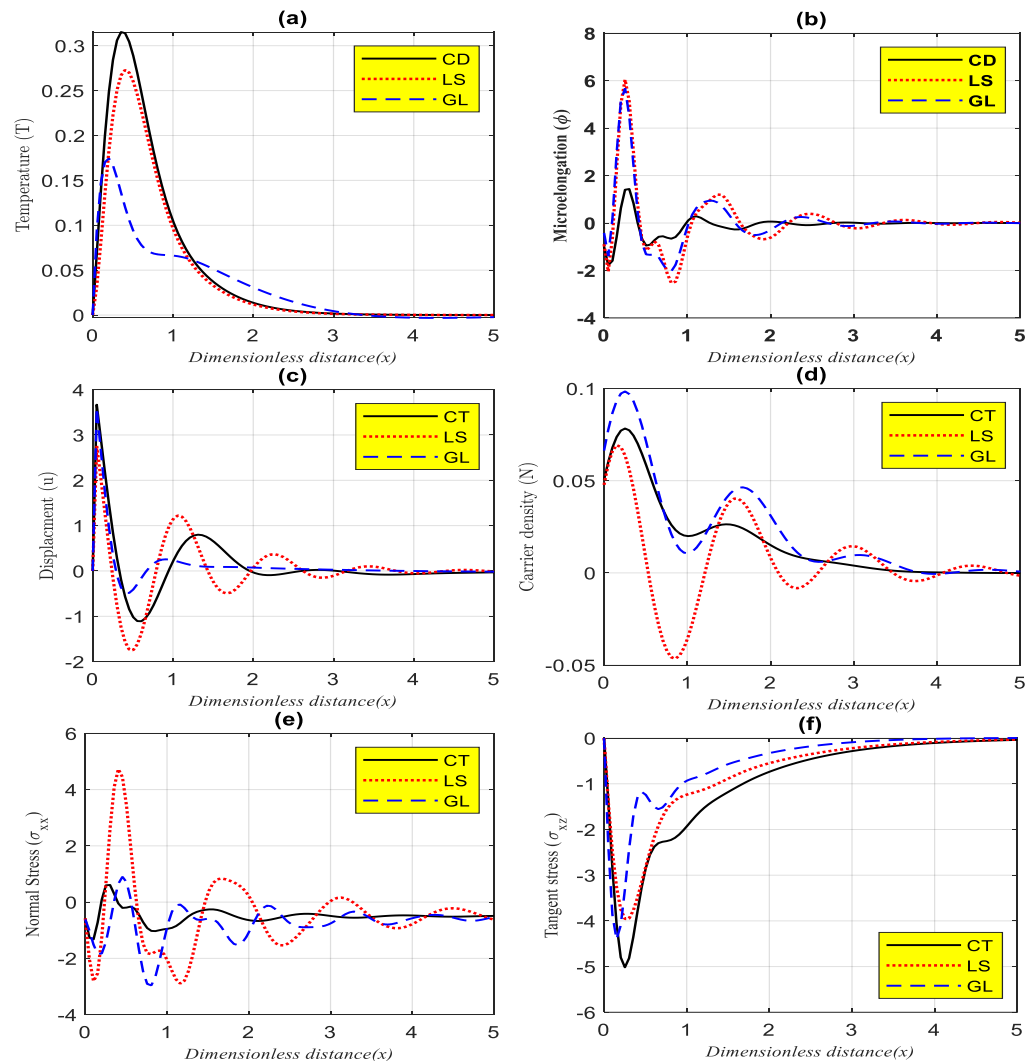
Unit	Symbol	Value	Unit	Symbol	Value
Nm <sup>-2</sup>	$\lambda$	$6.4 \times 10^{10}$	m <sup>3</sup>	$d_n$	$-9 \times 10^{-31}$
	$\mu$	$6.5 \times 10^{10}$			
kg/m <sup>3</sup>	$\rho$	2330	sec (s)	$\tau_0$	0.00005
K	$T_0$	800	m <sup>2</sup>	$j$	$0.2 \times 10^{-19}$
sec (s)	$\tau$	$5 \times 10^{-5}$	N	$\alpha_0$	$0.779 \times 10^{-9}$
K <sup>-1</sup>	$\alpha_{t_1}$	$0.04 \times 10^{-3}$	Nm <sup>-2</sup>	$\lambda_0$	$0.5 \times 10^{10}$
Wm <sup>-1</sup> K <sup>-1</sup>	$K_0$	150	Nm <sup>-2</sup>	$k$	$10^{10}$
J/(kg K)	$C_E$	695	Nm <sup>-2</sup>	$\lambda_1$	$0.5 \times 10^{10}$
m <sup>2</sup> /s	$D_E$	$2.5 \times 10^{-3}$	K <sup>-1</sup>	$\alpha_{t_2}$	$0.017 \times 10^{-3}$
m/s	$\tilde{s}$	2	m <sup>-3</sup>	$\tilde{n}_0$	$10^{20}$
H/m	$\mu_0$	$4\pi \times 10^{-7}$	sec (s)	$\nu_0$	0.0005
F/m	$\epsilon_0$	$8.85 \times 10^{-12}$	sec (s)	$t$	0.001

When the following parameters are selected without dimension, as in  $b = 1$  and  $\bar{p} = 2$  during a small time  $t = 0.001$  in the range  $0 \leq x \leq 5$  at  $z = -1$  and  $\omega = \omega_0 + i\zeta$  ( $\zeta = 0.05$  and  $\omega_0 = -2.5$ ), the transient waves in this simulation are graphed. On the other hand, the boundary surface conditions have an impact on the transient waves that are graphed.

According to the ED and TED, the principal physical distributions' wave propagation varies with the axial horizontal distance under the influence of variable thermal conductivity, and the magnetic field, as shown in Figure 1. According to the three different models CD, LS, and GL, the distributions of the thermal wave (temperature), microelongation wave function, and the elastic wave of displacement, carrier intensity in the context of the plasma wave, and the two mechanical waves  $\sigma_{xx}$  and  $\sigma_{xz}$  are investigated during the photo-thermoelasticity theory.  $n_0$  and  $n_1$  are two factors and thermal memory values that determine the three different models of photo-thermoelasticity.

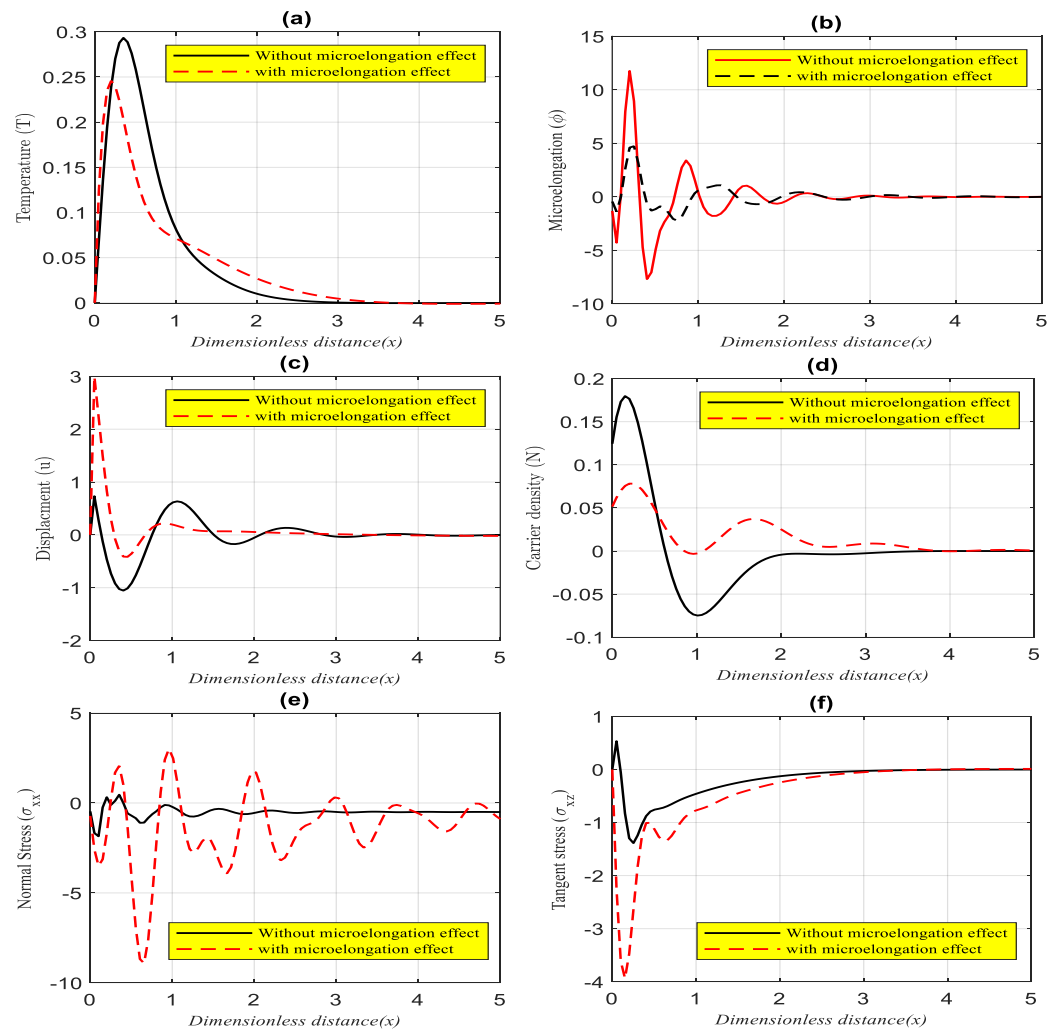
Figure 2 overall perspective shows that every physical quantity being studied satisfies the surface requirements of the microelongated semiconductor. The thermal wave (Figure 2a) and carrier density distribution start at zero and positive values, respectively, and increase in amplitude to reach their maximum values under the pressure force of the electromagnetic field and the thermal impact of light. The temperature distribution drops exponentially with wave behavior until it converges with the zero line as the distance grows, at which point it reaches its lowest value. However, the plasma wave (Figure 2d) in the second band exhibits a wave behavior, decreasing and increasing until it converges to the zero line. The two subfigures show that the thermal wave and plasma wave behaviors match those of the experiments reported in [51]. The microelongation wave propagation (Figure 2b), which starts at the surface from zero and declines in the closed initial range due to the magnetic pressure force and grows then decreases regularly with the wave behavior, can be used to characterize the microelongation scalar function. Due to the weak

magnetic field far from the semiconductor surface, the microelongation wave eventually converges to the zero line and establishes equilibrium inside the medium. The elastic wave (Figure 2c), which has a displacement component that can be defined, begins on the surface and rapidly rises as a result of an increase in particle vibrations caused by the magnetic field's pressure force and thermal stimulation to reach its maximum value. However, in the second range, the elastic wave alternates between periodic drops and increases as wave behavior spreads with the convergence of the zero line, eventually reaching the equilibrium state. The distribution of mechanical waves (Figure 2e) are represented by the tangent stress component  $\sigma_{xz}$  and normal stress component  $\sigma_{xx}$ . The normal distributions  $\sigma_{xx}$  decline in the first range, increase in the second range, and then regularly decrease and grow with wave behavior until they reach the equilibrium state. The tangent distribution  $\sigma_{xz}$ , (Figure 2f) on the other hand, starts at zero and decreases close to the surface until it approaches the minimal value. In the second range, as the distance increases, the tangent distribution  $\sigma_{xz}$  gradually grows until it hits the zero line (state of equilibrium). The wave propagations of the physical fields are impacted by the various relaxation time values. All of the subforms exhibit the same behavior for wave propagation processes with varied photothermal elasticity model values, but the extent of the differences depends on the values of the various relaxation times.



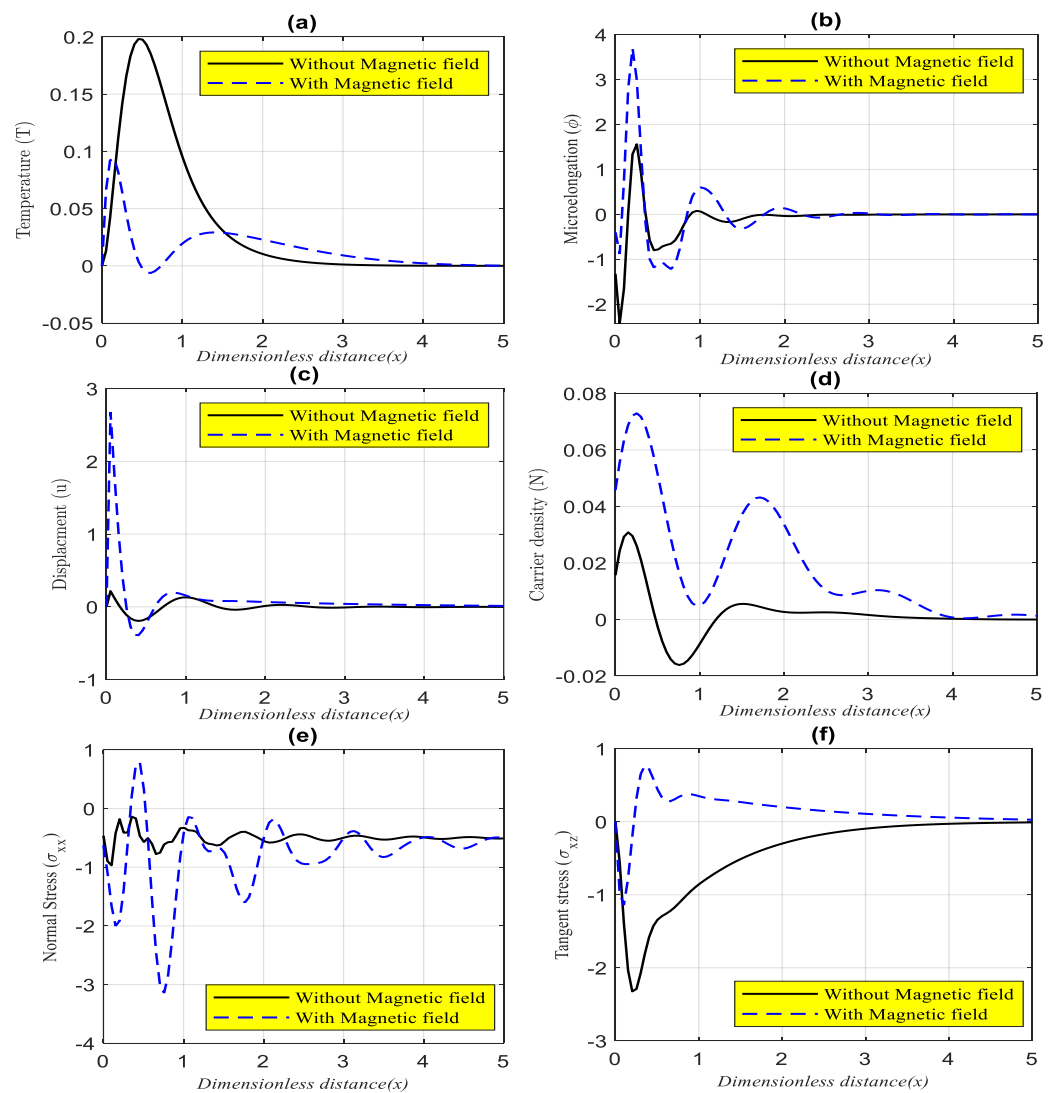
**Figure 2.** ((a) temperature distribution, (b) microelongation distribution, (c) displacement distribution, (d) carrier density distribution, (e) normal stress distribution, and (f) tangent stress distribution) The wave propagations of main physical fields with horizontal non-dimensional axis according to several microelongation-magneto-photo-thermoelasticity models.

Figure 3a–f compare the primary physical fields in two separate situations when a magnetic field was present at the same time for relatively brief periods. When the silicon material’s microelongation properties are disregarded, the first scenario is obtained. However, when the microelongation characteristics of the microelongated silicon material are taken into consideration, the second scenario is explored. According to the GL model, all calculations are carried out within the framework of the magneto-photo-thermoelasticity theory. This figure shows how the microelongation settings affect wave propagations and their magnitudes.



**Figure 3.** ((a) temperature distribution, (b) microelongation distribution, (c) displacement distribution, (d) carrier density distribution, (e) normal stress distribution, and (f) tangent stress distribution) The wave propagations of main physical fields with horizontal non-dimensional axis according to the GL model and a magnetic field both with and without microelongation parameters.

The behavior of wave propagations with distance in two situations is explained in Figure 4a–f. The first scenario demonstrates how the main physical fields change when a magnetic field is present (with a magnetic field). However, the second scenario demonstrates how the primary physical fields change when the magnetic field is absent (without the magnetic field). The GL model is used to implement the comparisons under the influence of microelongation parameters for the same short non-dimensional period. All wave propagations in all fields are significantly impacted by the magnetic field.



**Figure 4.** ((a) temperature distribution, (b) microelongation distribution, (c) displacement distribution, (d) carrier density distribution, (e) normal stress distribution, and (f) tangent stress distribution) The wave propagations of main physical fields with horizontal non-dimensional axis according to the GL model, as affected by microelongation parameters both with and without a magnetic field.

Figure 5a–f explain how wave propagation with distance behaves in three different circumstances. The first case shows how the main physical fields alter when thermal conductivity becomes temperature-independent. The second and third cases, on the other hand, show how the fundamental physical fields alter when the thermal conductivity is temperature-dependent. For the same brief non-dimensional period, comparisons are implemented using the GL model under the effect of microelongation parameters. The magnetic field has a substantial effect on all wave propagations in all fields.

Photothermal technology (PTT) is used in modern medicine as a non-invasive, selective treatment strategy for many different types of cancer. This technique is based on the conversion of light energy into heat on near-infrared laser irradiation. This is one of the most recent applications of this technology [52]. In modern industries, semiconductors are used to generate and store clean energy.

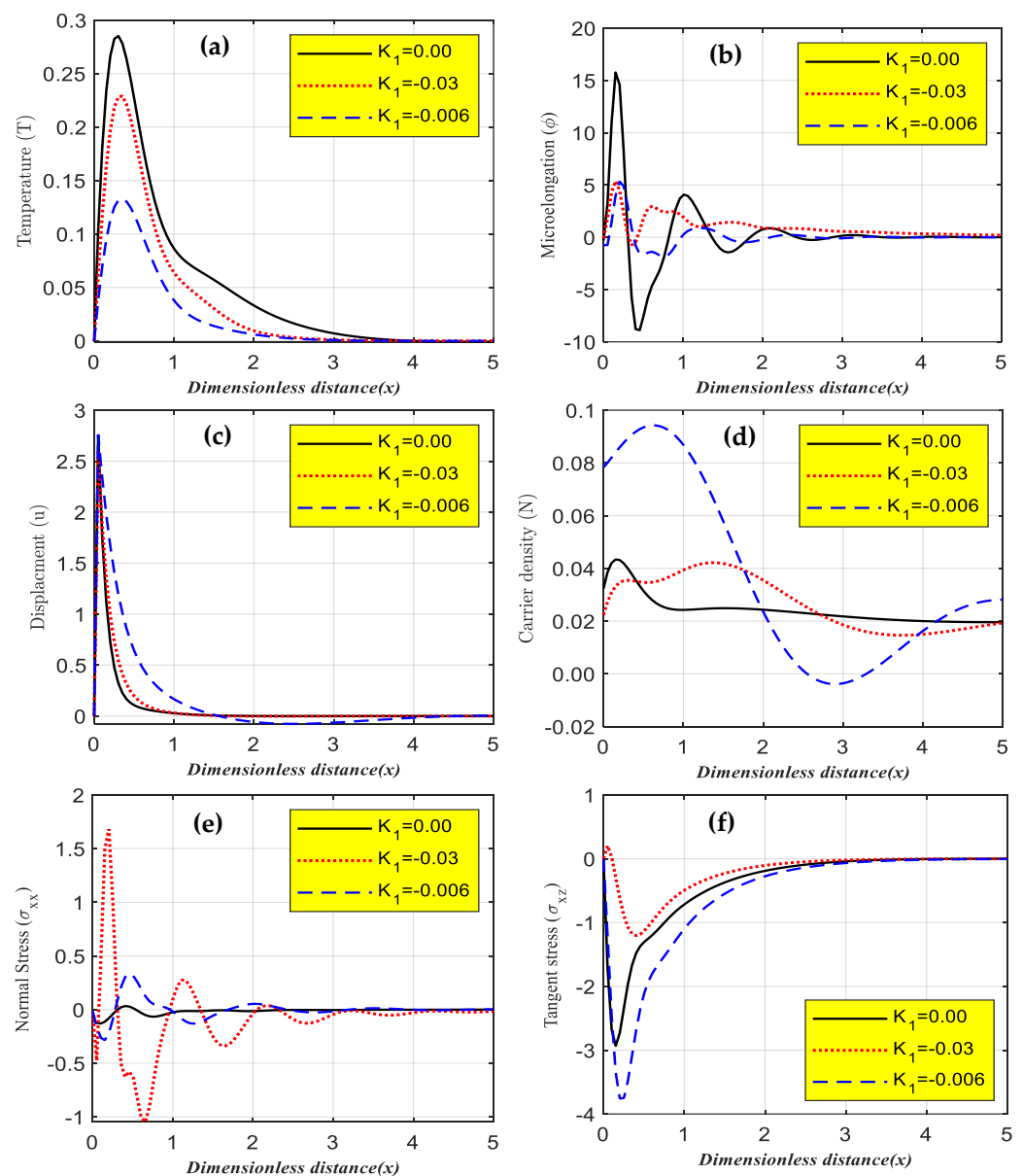


**Figure 5.** ((a) temperature distribution, (b) microelongation distribution, (c) displacement distribution, (d) carrier density distribution, (e) normal stress distribution, and (f) tangent stress distribution) The wave propagations of main physical fields with horizontal non-dimensional axis according to the GL model under the impact of the magnetic field, as affected by microelongation parameters with different values of variable thermal conductivity.

**7. Conclusions**

The photo-thermoelasticity theory is investigated when the microelongated semiconductor material is used, and a novel model is used to do so. When considering thermal-photo-excitation transport processes, the electromagnetic field is taken into consideration when the thermal conductivity is variable. According to the TD and TED with the modification of thermal memory, the governing equations describe the overlapping between the magneto-mechanical-thermal-plasma waves in 2D. According to the harmonic waves technique, the main equations are analyzed using the normal mode analysis. For the physical fields to reach an equilibrium condition, the wave distributions must disappear. The thermal memories that govern the CD, LS, and GL models are what determine how waves propagate. Therefore, the amplitude of wave propagation is greatly influenced by thermal memories. The wave propagation distributions are impacted by the microelongation factors.

On the other hand, the magnetic field increases the particle vibrations, which has an impact on how waves behave when electronics are deformed again. Many different industries, including sensors, medical devices, solar cells, and electrical circuits, use materials that are microelongated.

**Author Contributions:** Conceptualization, K.L.; methodology, K.L.; software, A.M.S. and A.A.E.-B.; validation, A.A.E.-B.; investigation, A.A.E.-B.; data curation, K.L.; writing—original draft preparation, A.M.S.; visualization, K.L.; supervision, K.L. All authors have read and agreed to the published version of the manuscript.

**Funding:** This research was funded by the Deputyship for Research & Innovation, Ministry of Education, Saudi Arabia, for funding this research work through the grant number (QU-IF-2-3-3-27075). The authors also thank to Qassim University for technical support.

**Institutional Review Board Statement:** Not applicable.

**Informed Consent Statement:** Not applicable.

**Data Availability Statement:** The datasets used and/or analyzed during the current study are available from the corresponding author on reasonable request.

**Acknowledgments:** The authors extend their appreciation to the Deputyship for Research & Innovation, Ministry of Education, Saudi Arabia, for funding this research work through the project number (QU-IF-2-3-3-27075). The authors also thank to Qassim University for technical support.

**Conflicts of Interest:** The authors declare no conflict of interest.

## Nomenclature

$\lambda, \mu$	Lame's parameters (N/m <sup>2</sup> ).
$\delta_n = (3\lambda + 2\mu)d_n$	Deformation potential difference (Nm).
$d_n$	Coefficient of ED (m <sup>3</sup> )
$T_0$	Reference temperature in its natural state (K)
$\hat{\gamma} = (3\lambda + 2\mu)\alpha_{t_1}$	Volume thermal expansion (NK/m <sup>2</sup> ).
$\sigma_{ij}$	Microelongational elastic stress (N/m <sup>2</sup> )
$\rho$	The density of the microelongated sample (kg/m <sup>3</sup> )
$\alpha_{t_1}$	Linear thermal expansion (K <sup>-1</sup> )
$n_0$	Equilibrium carrier concentration
$C_E$	Specific heat at constant strain (J/(kg K))
$K$	Thermal conductivity (Wm <sup>-1</sup> K <sup>-1</sup> )
$D_E$	Carrier diffusion coefficient (m <sup>2</sup> /s)
$\tau$	The lifetime of photogenerated carriers (s)
$E_g$	Energy gap (eV)
$e_{ij}$	Components of the strain tensor
$j_0$	Microinertia of microelement (m <sup>2</sup> )
$a_0, \alpha_0, \lambda_0, \lambda_1$	Microelongational material parameters (N, N, Nm <sup>-2</sup> , Nm <sup>-2</sup> )
$\tau_0, \nu_0$	Thermal relaxation times (s)
$\varphi$	Scalar microelongational function
$m_k$	Components of the microstretch vector
$s = s_{kk}$	Stress tensor component (N/m <sup>2</sup> )
$\delta_{ik}$	Kronecker delta
$\bar{s}$	Recombination velocities (m/s)

## References

1. Ghini, M.; Curreli, N.; Camellini, A.; Wang, M.; Asaithambi, A.; Kriegel, I. Photodoping of metal oxide nanocrystals for multi-charge accumulation and light-driven energy storage. *Nanoscale* **2021**, *13*, 8773. [[CrossRef](#)] [[PubMed](#)]
2. Almoneef, A.; El-Sapa, S.; Lotfy, K.; El-Bary, A.; Saeed, A. Laser Short-Pulse Effect on Thermodiffusion Waves of Fractional Heat Order for Excited Nonlocal Semiconductor. *Adv. Condens. Matter. Phys.* **2022**, *2022*, 1523059. [[CrossRef](#)]
3. Singh, R.; Singh, R.R. Optical properties of ZnS quantum dots: Applications in solar cells and biomedicine. *Biointerface Res. Appl. Chem.* **2022**, *13*, 158–167.

4. Li, J.-H.; Wu, J.; Yu, Y.-X. DFT exploration of sensor performances of two-dimensional WO<sub>3</sub> to ten small gases in terms of work function and band gap changes and I–V responses. *Appl. Surf. Sci.* **2021**, *546*, 149104. [[CrossRef](#)]
5. Amouami, E.I.; Perez, L.M.; Feddi, K.; El-Yadri, M.; Dujardin, F.; Suazo, M.J.; Laroze, D.; Courel, M.; Feddi, E. Influence of geometrical shape on the characteristic of the multiple InN/LnxGa1-xN quantum dot solar cells. *Nanomaterials* **2021**, *11*, 1317. [[CrossRef](#)] [[PubMed](#)]
6. Eringen, A.C. Microcontinuum Field Theories. In *Foundations and Solids*; Springer: New York, NY, USA, 1999; Volume 1.
7. Eringen, A.C. Linear theory of micropolar elasticity. *J. Math. Mech.* **1966**, *15*, 909–923.
8. Eringen, A.C. Theory of thermo-microstretch elastic solids. *Int. J. Eng. Sci.* **1990**, *28*, 1291–1301. [[CrossRef](#)]
9. Singh, B. Reflection and refraction of plane waves at a liquid/thermo-microstretch elastic solid interface. *Int. J. Eng. Sci.* **2001**, *39*, 583–598. [[CrossRef](#)]
10. Othman, M.; Lotfy, K. The influence of gravity on 2-D problem of two temperature generalized thermoelastic medium with thermal relaxation. *J. Comp. Theor. Nanosci.* **2015**, *12*, 2587–2600. [[CrossRef](#)]
11. Cicco, D.; Nappa, L. On the theory of thermomicrostretch elastic solids. *J. Therm. Stress.* **1999**, *22*, 565–580.
12. Othman, M.; Lotfy, K. On the plane waves of generalized thermo-microstretch elastic half-space under three theories. *Int. Comm. Heat Mass Trans.* **2010**, *37*, 192–200. [[CrossRef](#)]
13. Abouelregal, A.; Marin, M. The Size-Dependent Thermoelastic Vibrations of Nanobeams Subjected to Harmonic Excitation and Rectified Sine Wave Heating. *Mathematics* **2020**, *8*, 1128. [[CrossRef](#)]
14. Othman, M.; Lotfy, K. Effect of rotating on plane waves in generalized thermo-microstretch elastic solid with one relaxation time. *Multidis. Model. Mat. Str.* **2011**, *7*, 43–62. [[CrossRef](#)]
15. Ramesh, G.; Prasannakumara, B.; Gireesha, B.; Rashidi, M. Casson fluid flow near the stagnation point over a stretching sheet with variable thickness and radiation. *J. Appl. Fluid Mech.* **2016**, *9*, 1115–1122. [[CrossRef](#)]
16. Ezzat, M.; Abd-Elaal, M. Free convection effects on a viscoelastic boundary layer flow with one relaxation time through a porous medium. *J. Frankl. Inst.* **1997**, *334*, 685–706. [[CrossRef](#)]
17. Shaw, S.; Mukhopadhyay, B. Periodically varying heat source response in a functionally graded microelongated medium. *Appl. Math. Comput.* **2012**, *218*, 6304–6313. [[CrossRef](#)]
18. Shaw, S.; Mukhopadhyay, B. Moving heat source response in a thermoelastic micro-elongated Solid. *J. Eng. Phys. Thermophys.* **2013**, *86*, 716–722. [[CrossRef](#)]
19. Ailawalia, P.; Sachdeva, S.; Pathania, D. Plane strain deformation in a thermo-elastic microelongated solid with internal heat source. *Int. J. Appl. Mech. Eng.* **2015**, *20*, 717–731. [[CrossRef](#)]
20. Sachdeva, S.; Ailawalia, P. Plane strain deformation in thermoelastic micro-elongated solid. *Civ. Environ. Res.* **2015**, *7*, 92–98.
21. Ailawalia, P.; Kumar, S.; Pathania, D. Internal heat source in thermoelastic micro-elongated solid under Green Lindsay theory. *J. Theor. Appl. Mech.* **2016**, *46*, 65–82. [[CrossRef](#)]
22. Marin, M.; Lupu, M. On harmonic vibrations in thermoelasticity of micropolar bodies. *J. Vibrat. Control* **1998**, *4*, 507–518. [[CrossRef](#)]
23. Marin, M.; Stan, G. Weak solutions in Elasticity of dipolar bodies with stretch. *Carpath. J. Math.* **2013**, *29*, 33–40. [[CrossRef](#)]
24. Marin, M. Harmonic Vibrations in Thermoelasticity of Microstretch Materials. *J. Vib. Acoust. Trans. ASME* **2010**, *132*, 044501. [[CrossRef](#)]
25. Marin, M.; Othman, M.; Abbas, I. An extension of the domain of influence theorem for generalized thermoelasticity of anisotropic material with voids. *J. Comp. Theor. Nanosci.* **2015**, *12*, 1594–1598. [[CrossRef](#)]
26. Othman, M.; Said, S.; Marin, M. A novel model of plane waves of two-temperature fiber-reinforced thermoelastic medium under the effect of gravity with three-phase-lag model. *Int. J. Num. Meth. Heat Fluid Flow* **2019**, *29*, 4788–4806. [[CrossRef](#)]
27. Hobinya, A.; Alzahrani, F.; Abbas, I.; Marin, M. The effect of fractional time derivative of bioheat model in skin tissue induced to laser irradiation. *Symmetry* **2020**, *12*, 602. [[CrossRef](#)]
28. Gordon, J.P.; Leite, R.C.C.; Moore, R.S.; Porto, S.P.S.; Whinnery, J.R. Long-transient effects in lasers with inserted liquid samples. *Bull. Am. Phys. Soc.* **1964**, *119*, 501–510. [[CrossRef](#)]
29. Kreuzer, L.B. Ultralow gas concentration infrared absorption spectroscopy. *J. Appl. Phys.* **1971**, *42*, 2934. [[CrossRef](#)]
30. Tam, A.C. *Ultrasensitive Laser Spectroscopy*; Academic Press: New York, NY, USA, 1983; 108p.
31. Tam, A.C. Applications of photoacoustic sensing techniques. *Rev. Mod. Phys.* **1986**, *58*, 381. [[CrossRef](#)]
32. Tam, A.C. *Photothermal Investigations in Solids and Fluids*; Academic Press: Boston, MA, USA, 1989; 33p.
33. Hobinya, A.; Abbas, I. A GN model on photothermal interactions in a two-dimensions semiconductor half space. *Results Phys.* **2019**, *15*, 102588. [[CrossRef](#)]
34. Todorovic, D.M.; Nikolic, P.M.; Bojicic, A.I. Photoacoustic frequency transmission technique: Electronic deformation mechanism in semiconductors. *J. Appl. Phys.* **1999**, *85*, 7716–7726. [[CrossRef](#)]
35. Song, Y.Q.; Todorovic, D.M.; Cretin, B.; Vairac, P. Study on the generalized thermoelastic vibration of the optically excited semiconducting microcantilevers. *Int. J. Solids Struct.* **2010**, *47*, 1871. [[CrossRef](#)]
36. Lotfy, K. A novel model for Photothermal excitation of variable thermal conductivity semiconductor elastic medium subjected to mechanical ramp type with two-temperature theory and magnetic field. *Sci. Rep.* **2019**, *9*, 3319. [[CrossRef](#)] [[PubMed](#)]
37. Lotfy, K. Effect of Variable Thermal Conductivity during the Photothermal Diffusion Process of Semiconductor Medium. *Silicon* **2019**, *11*, 1863–1873. [[CrossRef](#)]

38. Alharthi, H.A. Characterization of the Vibration and Strain Energy Density of a Nanobeam under Two-Temperature Generalized Thermoelasticity with Fractional-Order Strain Theory. *Math. Comput. Appl.* **2021**, *26*, 78. [[CrossRef](#)]
39. Abbas, I.; Alzahrani, F.; Elaiw, A. A DPL model of photothermal interaction in a semiconductor material. *Waves Rand. Comp. Media* **2019**, *29*, 328–343. [[CrossRef](#)]
40. Khamis, A.; El-Bary, A.; Lotfy, K.; Bakali, A. Photothermal excitation processes with refined multi dual phase-lags theory for semiconductor elastic medium. *Alex. Eng. J.* **2020**, *59*, 1–9. [[CrossRef](#)]
41. Lotfy, K. A novel model of magneto photothermal diffusion (MPD) on polymer nano-composite semiconductor with initial stress. *Waves Ran. Comp. Med.* **2021**, *31*, 83–100. [[CrossRef](#)]
42. Alzahrani, F.S.; Abbas, I. Photo-Thermal Interactions in a Semiconducting Media with a Spherical Cavity under Hyperbolic Two-Temperature Model. *Mathematics* **2020**, *8*, 585. [[CrossRef](#)]
43. Lotfy, K.; Kumar, R.; Hassan, W.; Gabr, M. Thermomagnetic effect with microtemperature in a semiconducting Photothermal excitation medium. *Appl. Math. Mech. Engl. Ed.* **2018**, *39*, 783–796. [[CrossRef](#)]
44. Yadav, A. Photothermal plasma wave in the theory of two-temperature with multi-phase-lag thermo-elasticity in the presence of magnetic field in a semiconductor with diffusion. *Waves Random Complex Media* **2022**, *32*, 2416–2444. [[CrossRef](#)]
45. Lotfy, K.; Hassan, W.; El-Bary, A.; Kadry, M. Response of electromagnetic and Thomson effect of semiconductor medium due to laser pulses and thermal memories during photothermal excitation. *Results Phys.* **2020**, *16*, 102877. [[CrossRef](#)]
46. Mun, J.; Ochiai, Y.; Wang, W.; Zheng, Y.; Zheng, Y.Q.; Wu, H.C.; Matsuhisa, N.; Higashihara, T.; Tok, J.B.; Yun, Y.; et al. A design strategy for high mobility stretchable polymer semiconductors. *Nat Commun.* **2021**, *12*, 3572. [[CrossRef](#)] [[PubMed](#)]
47. Lord, H.; Shulman, Y. A generalized dynamical theory of thermoelasticity. *J. Mech. Phys. Solid.* **1967**, *15*, 299–309. [[CrossRef](#)]
48. Green, A.; Lindsay, K. Thermoelasticity. *J. Elast.* **1972**, *2*, 1–7. [[CrossRef](#)]
49. Biot, M. Thermoelasticity and irreversible thermodynamics. *J. Appl. Phys.* **1956**, *27*, 240–253. [[CrossRef](#)]
50. Mandelis, A.; Nestoros, M.; Christofides, C. Thermoelectronic-wave coupling in laser photothermal theory of semiconductors at elevated temperatures. *Opt. Eng.* **1997**, *36*, 459–468. [[CrossRef](#)]
51. Liu, J.; Han, M.; Wang, R.; Xu, S.; Wang, X. Photothermal phenomenon: Extended ideas for thermophysical properties characterization. *J. Appl. Phys.* **2022**, *131*, 065107. [[CrossRef](#)]
52. Han, H.S.; Choi, K.Y. Advances in Nanomaterial-Mediated Photothermal Cancer Therapies: Toward Clinical Applications. *Biomedicines* **2021**, *9*, 305. [[CrossRef](#)]